Neural network architectures for Schizophrenia patients-versus-Controls classification based on Amygdala connectivity.

Authors: Majnu John[a, *], Janina Ferbinteanu[b], Tossi Ikuta[c]

[a] Institute of Behavioral Neuroscience, Feinstein Institutes of Medicine, NorthWell Health, Manhasset, NY.

[b] Department of Neurobiology and Behavior, UC Irvine, Irvine, CA.

[c] Department of Communication Sciences and Disorder, University of Mississippi, Oxford, MS.

* Corresponding Author:

Toshikazu Ikuta, Department of Communication Services and Disorders, University of Mississippi, USA. E-mail address: tikuta@olemiss.edu

Detailed Methods

In this short note, we present results from analysis utilizing classification methods based on deep neural networks and convolutional neural networks for predicting schizophrenia versus healthy control using amygdala's connectivity to other brain regions. The predictor data consisted of rs-fMRI data tensors of shape 91 x 109 x 91 where each voxel represented Z-score of connectivity to amygdala. The MRI images and the target binary classification variable from the Center for Biomedical Research Excellence in Brain Function and Mental Illness (Cetin et al., 2014) were obtained from Collaborative Informatics and Neuroimaging Suite (http://coins.mrn.org/). Excluding the bipolar patients from the original sample resulted in a total of 173 subjects for the current analysis, with 90 control subjects and 83 patients with schizophrenia or schizoaffective disorder. Resting state echo planner image (EPI) volumes had 32 slices of 4 mm 64x64 matrix with 4-mm thickness (voxel size = 3x3x4 mm), with repetition time (TR) of 2000 milliseconds and echo time (TE) of 29 milliseconds. A total of 150 volumes (5 minutes) were used in the analysis. High-resolution structural T1 volume was acquired as 176 sagittal slices of 256 mm x 256 mm with 1-mm thickness (voxel size = 1x1x1 mm, TR=2530 milliseconds and TE=3.25 milliseconds). Data preprocessing was conducted using FMRIB Software Library (FSL) using procedures very similar to the steps described in Kiparizoska and Ikuta, 2017.

FMRIB Software Library (FSL,) as well as Analysis of Functional NeuroImages (AFNI) were used for data preprocessing. The structural T1 volume for each subject was skull stripped, segmented (gray matter, white matter and CSF), and registered to the MNI 2mm standard brain. After removing first four EPI volumes transient signal spikes were removed by de-spiking interpolation. Head motion was corrected by linearly registering all the volumes to the first volume, through which six motion parameters and displacement distance between two consecutive volumes were estimated. Eac volumes was regressed by white matter and cerebrospinal fluid signal fluctuations

as well as the six motion parameters. EPI volumes were smoothed with a 6mm FWHM Gaussian kernel, resampled and then spatially transformed, and aligned to the MNI 2mm standard brain space through which12 affine parameters were created between rs-fMRI volume and MNI152 2mm space, so that a seed ROI can later be registered to each individual rs-fMRI space. In order to detect excess motion, the root mean square deviation was calculated from motion correction parameters, at an *r=40mm* spherical surface using FSL's *rmsdiff* tool (Power et al., 2012, 2014). Volumes were removed if displacement distance exceeded the threshold (0.3mm) (i.e., *scrubbed*) from further statistical analyses (Siegel et al., 2014).

Functional connectivity of the amygrala was tested by testing every voxel in the whole brain tested by ADNI's *3dROIstats*, using amygdala ROI defined by Harvard_Oxford atlas (Makris et al 2006). The Z-scores were calculated by AFNI's *3dcalc*, then registered to the MNI2mm space. Functions in the nibabel Python module were utilized to read in the images and convert them into tensors for neural network inputs. Python modules numpy and tensorflow and Keras API were utilized to further process the data and implement the neural network models.

We present results from three different neural network architectures – 1) deep neural network (DNN), 2) a linear convolutional neural network (CNN) and 3) RESNET-34 which is a nonlinear CNN architecture. Our DNN consisted of 5 hidden layers with 4096 nodes in addition to input and output layers. Our linear CNN is an adaptation of the CNN architecture presented in chapter 14 in Geron, 2019. It consisted of two convolutional layers with batch normalization and max-pooling layers in between. The number of square filters (- of sizes 3 and 2, respectively-) in the first and second convolutional layers were 64 and 128. The output from the second convolutional layer was flattened and then transitioned through 5 dense layers, each with 512 nodes. The dense layers were interspersed with dropout-regularization layers with 50% dropout-probability. ResNet-34 is the standard residual learning architecture with 34 layers containing 3 residual units that output 64 feature maps, 4 residual units with 128 maps, 6 residual units with 256 maps, and 3 residual units with 512 maps. The activation function used for all layers (convolutional and dense) in all three architectures was ReLU. The optimizer used for DNN was stochastic gradient descent (SGD), and for linear CNN and RESNET-34 was 'Adam', a variant of SGD. 30 epochs were used for training the first two architectures and 300 epochs used for the ResNet-34 architecture. Performance for all architectures was assessed using random-shuffle cross-validation (CV) with 25 iterations. For each iteration, the 173 samples were split randomly into training, validation and test sets of 120, 18 and 35 samples respectively. Median and inter-quartile range (IQR) values of the accuracy rates are presented as results below. The Python codes and the Jupyter-Notebook output for all analyses are posted in 'https://github.com/mjohn5/amygdalaconnectivity'.

Results

Median accuracy rate (and IQR) of the DNN architecture based on 25 CV-iterations were 62.9% (60.0%, 65.7%). The median accuracy rate for both the CNN and ResNet architectures was 60.0% with corresponding IQRs being (57.1%, 62.9%) and (57.1%, 65.7%), respectively. The results are graphically represented in the figure below.

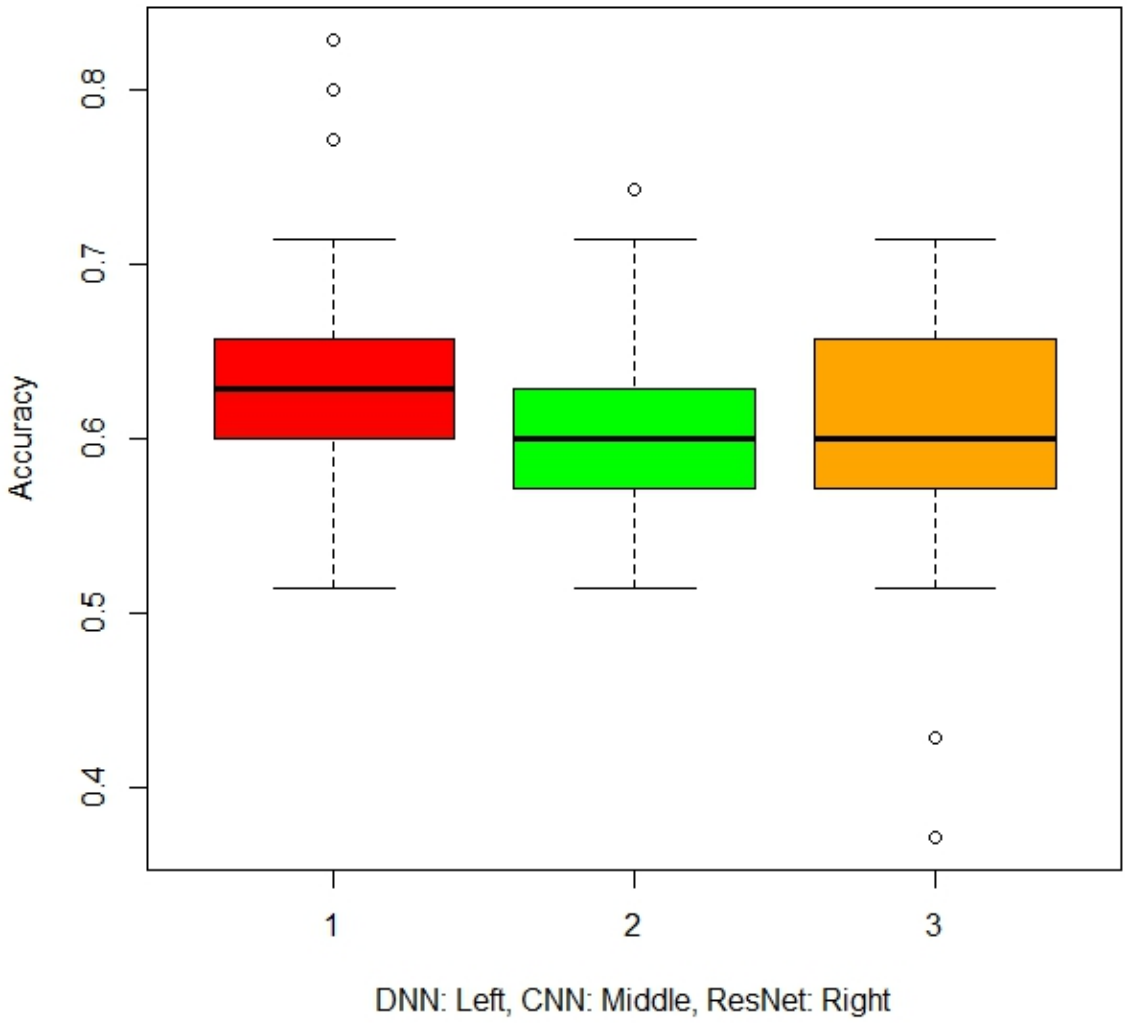

References

Çetin MS, Christensen F, Abbott CC, Stephen JM, Mayer AR, Cañive JM, Bustillo JR, Pearlson GD, Calhoun VD. Thalamus and posterior temporal lobe show greater inter-network connectivity at rest and across sensory paradigms in schizophrenia. Neuroimage. 2014 Aug 15;97:117-26. doi: 10.1016/j.neuroimage.2014.04.009.

Geron A. *Hands-On Machine Learning with Scikit-Learn & TensorFlow*. 2nd ed: O-Reilly Media Inc; 2019.

Kiparizoska S, Ikuta T. Disrupted Olfactory Integration in Schizophrenia: Functional Connectivity Study. Int J Neuropsychopharmacol. 2017 Sep 1;20(9):740-746. doi: 10.1093/ijnp/pyx045.

Makris N, Kaiser J, Haselgrove C, Seidman LJ, Biederman J, Boriel D, Valera EM, Papadimitriou GM, Fischl B, Caviness VS, Kennedy DN, 2006. Human cerebral cortex: a system for the integration of volume and surface-based representations. NeuroImage 33, 139–153.

Power JD, Barnes KA, Snyder AZ, Schlaggar BL, Petersen SE. Spurious but systematic correlations in functional connectivity MRI networks arise from subject motion. Neuroimage. 2012 Feb 1;59(3):2142-54. doi: 10.1016/j.neuroimage.2011.10.018. Epub 2011 Oct 14. Erratum in: Neuroimage. 2012 Nov 1;63(2):999. PMID: 22019881; PMCID: PMC3254728.

Power JD, Mitra A, Laumann TO, Snyder AZ, Schlaggar BL, Petersen SE. Methods to detect, characterize, and remove motion artifact in resting state fMRI. Neuroimage. 2014 Jan 1;84:320-41. doi: 10.1016/j.neuroimage.2013.08.048. Epub 2013 Aug 29. PMID: 23994314; PMCID: PMC3849338.

Siegel JS, Power JD, Dubis JW, Vogel AC, Church JA, Schlaggar BL, Petersen SE. Statistical improvements in functional magnetic resonance imaging analyses produced by censoring high-motion data points. Hum Brain Mapp. 2014 May;35(5):1981-96. doi: 10.1002/hbm.22307. Epub 2013 Jul 17. PMID: 23861343; PMCID: PMC3895106.